Front. Optoelectron. 2019, 12(4): 405–412
https://doi.org/10.1007/s12200-019-0865-x

RESEARCH ARTICLE

Experimental and simulation assessments of underwater light propagation

Fatah ALMABOUADA (✉)[1,2], Manuel Adler ABREU[3], João M. P. COELHO[3], Kamal Eddine AIADI[4]

1 Faculté des Mathématiques et des Sciences de la Matière, Département de Physique, Univérsité Kasdi Merbah Ouargla, Ouargla 30000, Algérie
2 Centre de Développement des Technologies Avancées, Division Milieux Ionisés & Lasers, Alger 16303, Algérie
3 Laboratório de Óptica, Laser e Sistemas, Faculdade de Ciências da Universidade de Lisboa Campus do Lumiar, Estrada do Paço do Lumiar, Lisboa 1649-038, Portugal
4 Faculté des Mathématiques et des Sciences de la Matière, Laboratoire LENREZA, Univérsité Kasdi Merbah Ouargla, Ouargla 30000, Algérie

Abstract This paper investigates the light propagation through several types of water by experimental and simulation. The Zemax-ray tracing software allowed to simulate the propagation of light in water and to observe the receiver response by reproducing the real conditions of propagation. The underwater environment has been reproduced by a 1.2 m long water tube and 20 cm in diameter with a glass window fitted on one side. The use of tap water with different amounts of sand leads toward three types of water with different attenuation coefficients (0.133, 0.343, 0.580 m^{-1}). The light transmission in the three types of water was experimentally evaluated using a doubled Nd:YAG laser with energy of 4.3 mJ and a pulse width of 20 ns. Comparisons were done between simulation and experimental results.

Keywords underwater light propagation, attenuation coefficient, telescope, laser range finder

1 Introduction

Since several decades, sound waves have been used in underwater ranging techniques [1]. This allowed the development of several applications, such as sea bed structure [2], bathymetry and imaging [3,4]. Nowadays, laser sources are used in underwater for imaging [5,6], scanning [7], predicting water turbidity [8], underwater laser induced breakdown spectroscopy (LIBS) [9], remote sensing [10], and obstacle detection [11].

An underwater time of flight laser range finder [12] requires a receiver channel to achieve the ranging measurement. This receiver comprises a telescope and a photo-detector. The goal of the telescope is to focus the reflected optical signal on the active area of the photo-detector [13,14]. This latter converts the optical signal to photo-current.

This paper is a contribution to the state-of-the-art in the study of the transmission of light in water media through simulation and experiment.

Section 2 of this paper describes the parameters influencing the light propagation in water and the water types used in the assessment. In Section 3, the simulation results of underwater light transmission are presented. In Section 4, the experimental results are discussed. Finally, concluding remarks are given in Section 5.

2 Method and experimental setup

The water environment is characterized by its attenuation coefficient which is several times higher than in the atmosphere. Therefore, for long distances of propagation in water, the appropriate wavelengths are the blue and green ones [15,16].

The attenuation coefficient $c(\lambda)$, where λ refers to the wavelength of light, is the decay constant associated with the removal of light intensity as given by Eq. (1) [17].

$$I(z) = I(0)\exp\Big(-c(\lambda)\cdot z\Big), \tag{1}$$

where z is the distance of propagation, $I(0)$ and $I(z)$ are respectively the intensities at position $z = 0$ and $z = z$.

As reported in Table 1 [16], this coefficient varies from one water type to another, such as turbid harbor, coastal ocean, and clear ocean [18].

To reproduce experimentally an underwater environment with different kinds of water as in Table 1, we use tap

Received August 2, 2018; accepted December 2, 2018

E-mail: falmabouada@cdta.dz

water with different amounts of sand. Two amounts of sand were added to the water: 250 and 350 g. A scanning electron microscopy (SEM) allowed to specify the particle sizes of sand in the range of 100 to 400 μm. The attenuation coefficients of three types of water defined as W1, W2, and W3 were experimentally determined similarly to the work of Boivin et al. [19]. As summarized in Table 2, the attenuation coefficient of tap water W1 is 0.130 m^{-1}, which corresponds approximately to that of clear ocean. Besides, the attenuation coefficient of tap water plus 250 g of sand W2 takes the value of 0.343 m^{-1} that is nearly close to that of coastal ocean (0.348 m^{-1}) according to Sverdrup et al. [20]. Finally, the attenuation coefficient of tap water plus 350 g of sand W3 is 0.580 m^{-1}, which probably corresponds to the lowest turbid harbor water since nowhere similar value has been reported for coastal water at 532 nm.

The underwater environment is reproduced by 1.2 m long water tube and 20 cm in diameter with a glass window fitted on one side. For each water type, the experiment is performed with an intra-cavity frequency-doubling of a Nd:YAG laser passively Q-switched to generate the 532 nm wavelength. The output laser energy is 4.3 mJ for a pulse width of 20 ns at a repetition rate of 1 Hz. This corresponds to a peak power of 2.15 $\times 10^5$ W.

Table 1 Attenuation coefficient of several types of water at $\lambda = 530$ nm

water type	c/m^{-1}
clear ocean	0.151
coastal ocean	0.398
turbid harbor	2.190

Table 2 Attenuation coefficients of the three types of water at $\lambda = 530$ nm

water type	c/m^{-1}
W1: tap water	0.130
W2: tap water + 250 g of sand	0.343
W3: tap water + 350 g of sand	0.580

3 Simulation of underwater light propagation

The Zemax-ray tracing software [21,22] is used to reproduce the receiving telescope and to simulate the propagation of light in the real environment of propagation. As shown in Fig. 1(a), the arrangement of the receiving telescope is achieved in the sequential mode of Zemax [23]. It is constituted of an objective (Plano-convex lens with a diameter D = 50 mm and a focal length FL = 100 mm), a Bi-concave lens (D = 45 mm, FL = –50 mm), and a Plano-convex lens (D = 25 mm, FL = 35 mm). As observed in Fig. 1(b), the received laser rays are focused inside the active area (diameter of 800 μm) of the photodetector. The 3-D profile of the telescope is illustrated in Fig. 2.

To observe the light transmission through the different water types, the telescope is translated to the non-sequential mode (NSC) of Zemax [21]. According to the experimental conditions, the water media is reproduced in 1.2 m water tank in length and situated 5 m far from the telescope. For each water type presented in Table 2 and the turbid harbor (Table 1), the attenuation coefficient is considered to evaluate the laser power arriving at the object. This evaluation is necessary in Zemax because the object is considered as the laser source. Considering the attenuation coefficient of one travel of the laser source through each water type, the reflected laser power being reflected by the object is evaluated by Eq. (1). The parameters used in the NSC simulations are summarized in Table 3.

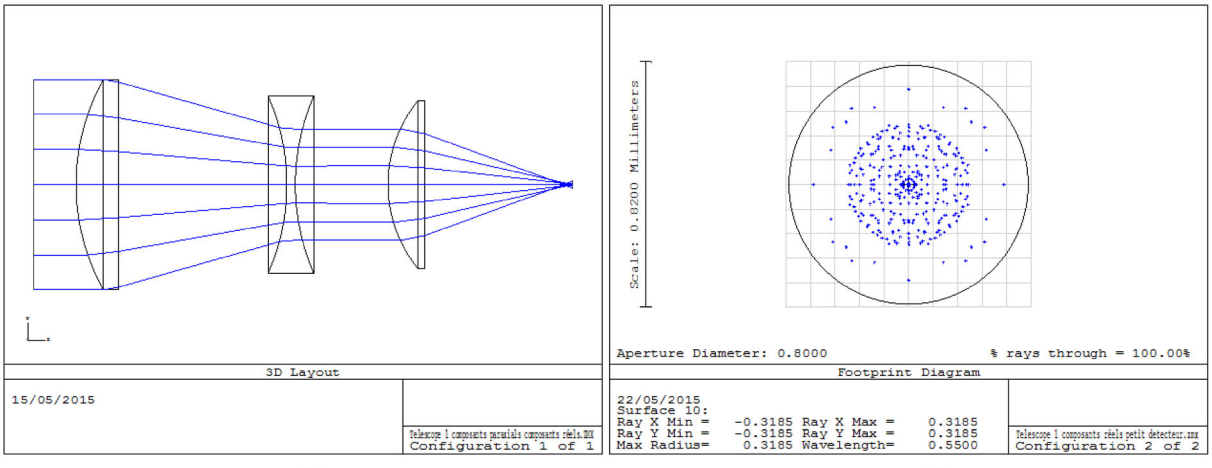

(a) (b)

Fig. 1 Designed telescope (a) under Zemax software and (b) the detector area window

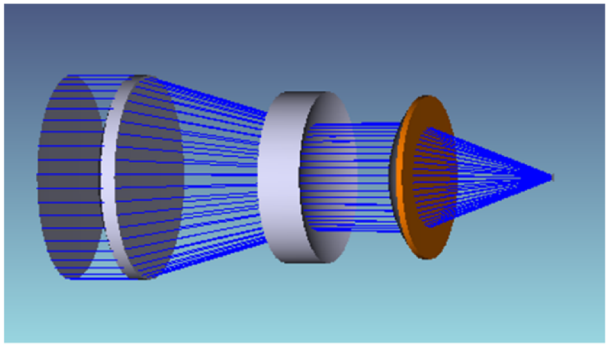

Fig. 2 3-D profile of the receiving telescope

Table 3 Numerical values of parameters and constants for Zemax simulation

parameter	value
laser wavelength/nm	532
transmitted laser power p_{out}/W	2.15 $\times 10^5$
estimated laser power at the object/ $\times 10^5$ W	1.83, 1.42, 1.07, 0.155
attenuation coefficient of water/m^{-1}	0.130, 0.343, 0.580, 2.190
estimated laser beam diameter at the object/mm	4.36
diameter of the telescope objective D_{opt}/m	0.05
distance between the object and telescope/m	5 (air) + 1.2 (water)
detector active area diameter/μm	800
temperature of water/°C	20

The 2-D and 3-D profiles of the simulated laser source are displayed in Fig. 3. In the window of the 2-D profile, the color bar represents the peak irradiance (W/cm^2).

The first simulation was done for water type W1 with an attenuation coefficient of 0.130 m^{-1}. Figure 4 depicts the 2-D and 3-D profiles of the reflected laser beam recorded on the detector area. The collected laser power is equal to 1.17 $\times 10^5$ W, which corresponds to 54.4% of the laser source power (2.15 $\times 10^5$ W) as seen in Fig. 4(b).

In the case of water type W2, corresponding to the increase of the attenuation coefficient from 0.130 to 0.343 m^{-1}, the obtained 2-D and 3-D profiles of the reflected laser beam are illustrated in Figs. 5(a) and 5(b). The transmitted laser power is of 6.8 $\times 10^4$ W, which represents 31.4% of the laser source power. Under such conditions, the attenuation is more important since we observe a decrease of the reflected power versus the increase of the attenuation coefficient of water.

The third simulation was performed for water type W3 representing the attenuation coefficient of 0.580 m^{-1}. The 2-D and 3-D profiles of the reflected laser beam are displayed in Figs. 6(a) and 6(b). The transmitted laser power is about 3.72 $\times 10^4$ W, which corresponds to 17.3% of the laser source power.

The last simulation was done for turbid harbor water as reported in Table 1. Figure 7 depicts the 2-D and 3-D profiles of the transmitted laser light. The laser power as shown in the detector area is equal to 979 W, which corresponds to 0.45% of the transmitted laser power (2.15 $\times 10^5$ W) as seen in Fig. 7(b). For this water type, the transmitted laser light is strongly attenuated comparing with the others simulated water types. This is the fact of the attenuation coefficient which is higher (2.190 m^{-1}) than the others attenuation coefficients (0.130, 0.343, 0.580 m^{-1}) of the specified types of water.

One can observe from the recorded profiles that the received laser powers decrease with the increase of the attenuation coefficient of water. Also, the laser beam size as seen by the telescope is practically the same. This last fact reflects directly on the optimization of the detector area and on the magnification of the telescope. However, we should note that increasing the active area of the detector may have a negative impact on the increase of the noise of the system. A detector with larger area will show more intrinsic noise and will increase the effective field of view

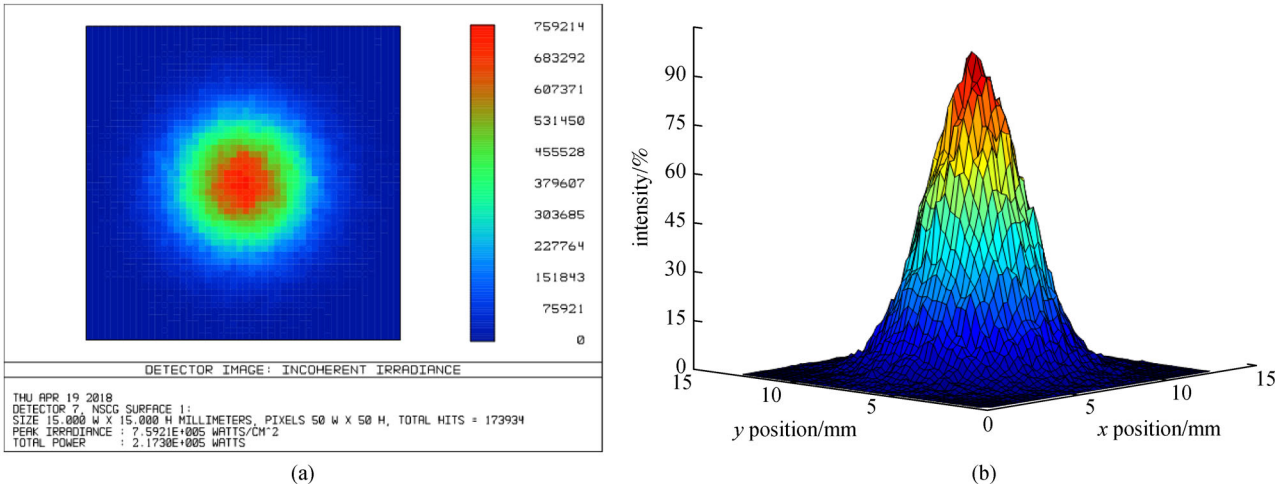

Fig. 3 (a) 2-D and (b) 3-D profiles of the laser source

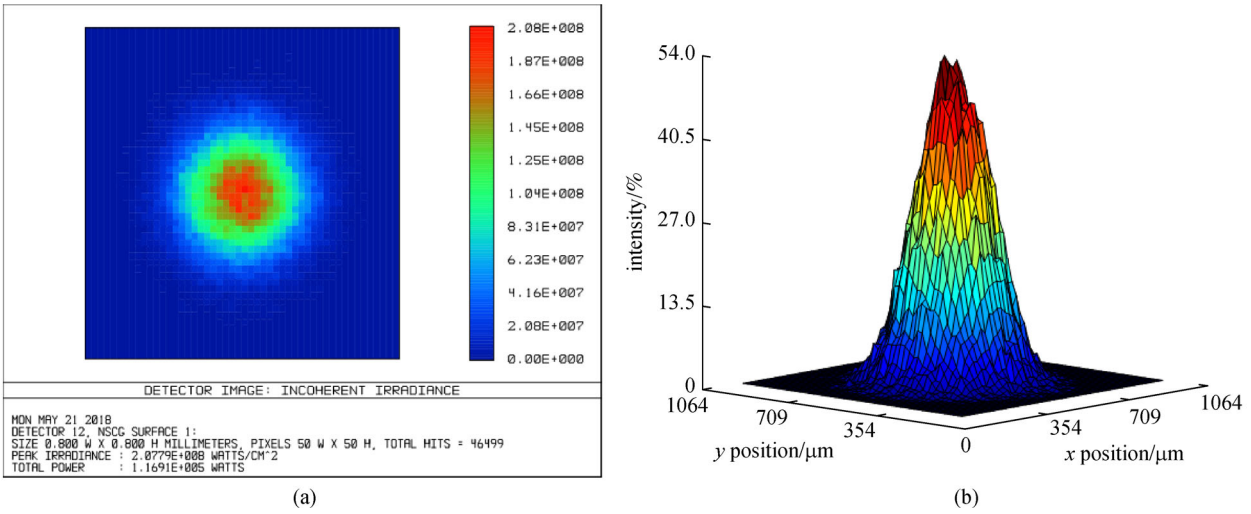

Fig. 4 (a) 2-D and (b) 3-D profiles of the reflected laser beam recorded in the detector area for W1

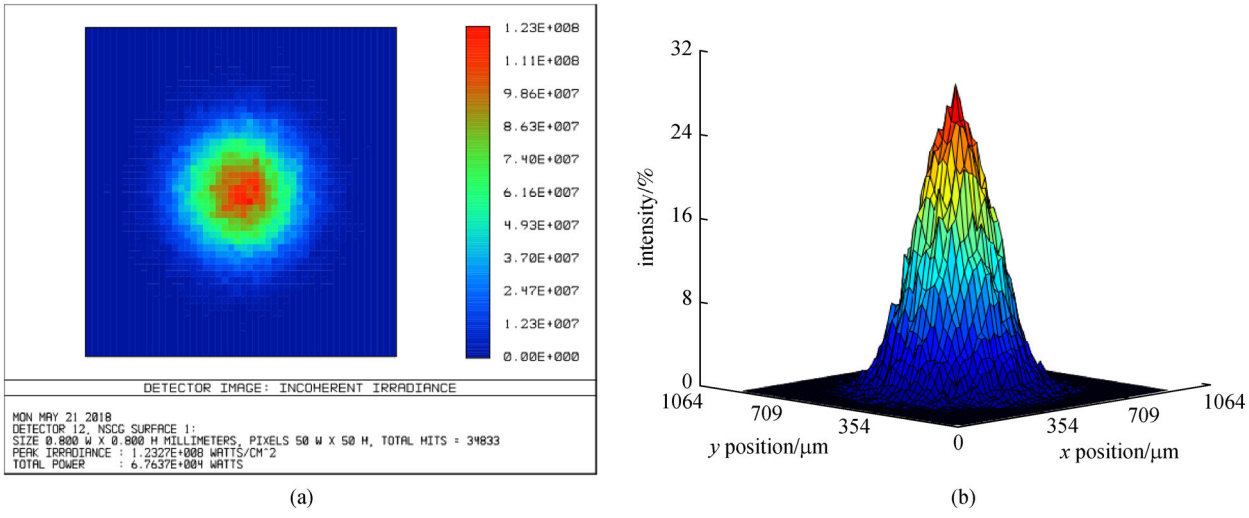

Fig. 5 (a) 2-D and (b) 3-D profiles of the reflected laser beam recorded in the detector area for W2

of the detector, making it more exposed to the background radiation.

4 Experimental results

The experimental setup is shown in Fig. 8. The laser source is oriented to the glass window of the water tube situated 5 m far. A Teflon (PTFE) cube (70×70×70 mm^3) is immersed in water through a hole about 12 cm in diameter. The cube has a reflection coefficient of up to 98% in the wavelength range of 250 to 2500 nm. The telescope presented in the previous section was achieved and positioned parallel to the laser source to collect the reflected laser beam from the object. A charge coupled device (CCD) camera records the reflected laser beam profiles at the output of the telescope. This camera has a sensor size of 6.16 ×4.62 mm^2, a video resolution of 1280×720 pixels (high quality) and an optical zoom 5 ×. The 2-D and 3-D profiles of the laser spot are displayed on the computer screen.

The 2-D and 3-D profiles of the *Q*-switched laser source are depicted in Figs. 9(a) and 9(b).

Figures 10(a) and 10(b) depict the 2-D and 3-D profiles of the reflected laser beam obtained in case of water type W1 at a temperature of 20°C (293 K). These profiles look like the laser source profiles (Figs. 9(a) and 9(b)) with a certain attenuation of intensity due to the propagation in water. The received laser power at the output of the telescope is of 1.22 $\times 10^5$ W, which corresponds to 57% of the laser source power (2.15 $\times 10^5$ W). This value is nearly close to that of simulated one (1.17 $\times 10^5$ W) for the same water type (Fig. 4). As shown in the 2-D profile, the beam spot diameter is under 800 μm.

In the second experiment with water type W2, the 2-D

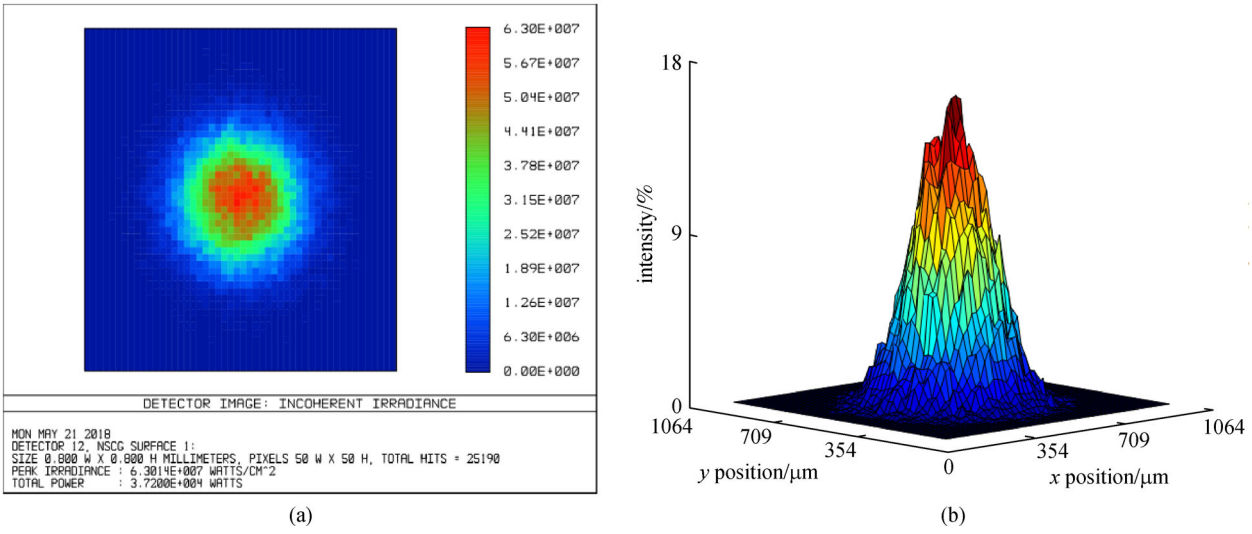

Fig. 6 (a) 2-D and (b) 3-D profiles of the reflected laser beam recorded in the detector area for W3

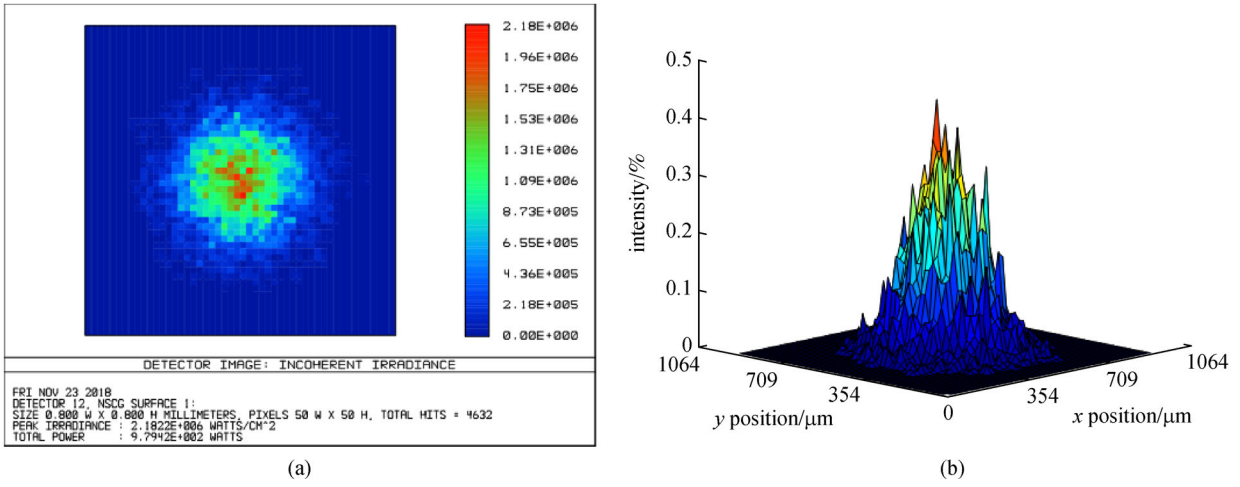

Fig. 7 (a) 2-D and (b) 3-D profiles of the reflected laser beam recorded in the detector area for turbid harbor

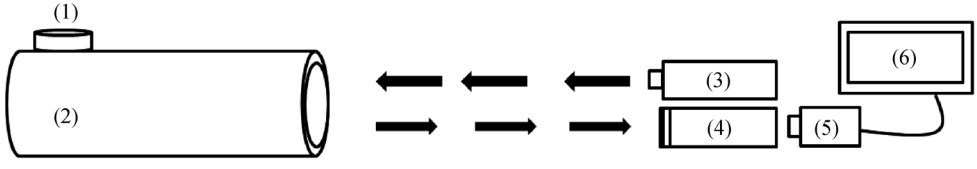

Fig. 8 Experimental setups. (1) Hole; (2) water tank; (3) *Q*-switched Nd:YAG laser; (4) telescope; (5) CCD camera; (6) screen

and 3-D profiles of the reflected laser beam are shown in Figs. 11(a) and 11(b). As expected, the intensity is less than that in case of W1 (Figs. 10(a) and 10(b)). The reflected laser power is of 6.15×10^4 W, which corresponds to 28.6% of the laser source power. This value is nearly close to that of simulated one (6.8×10^4 W) for the same water W2.

In the last experiment with water type W3, the reflected 2-D and 3-D profiles are depicted in Figs. 12(a) and 12(b). Here, the attenuation is more pronounced as expressed by the decrease of the reflected laser power due to the increase of the amount of sand from 250 to 350 g. The reflected power is of 3.65×10^4 W, which corresponds to 17% of the laser source power. This value is the same to that obtained by simulation (3.72×10^4 W) in case of W3.

In summary, the transmitted laser powers recorded from simulation and experiment are approximately the same for

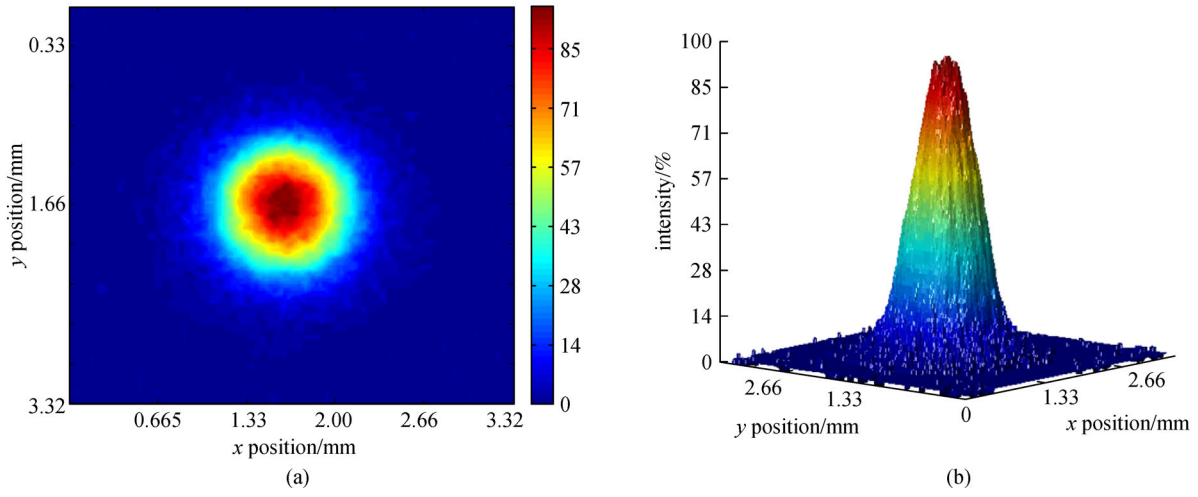

Fig. 9 (a) 2-D and (b) 3-D beam profiles of the laser source

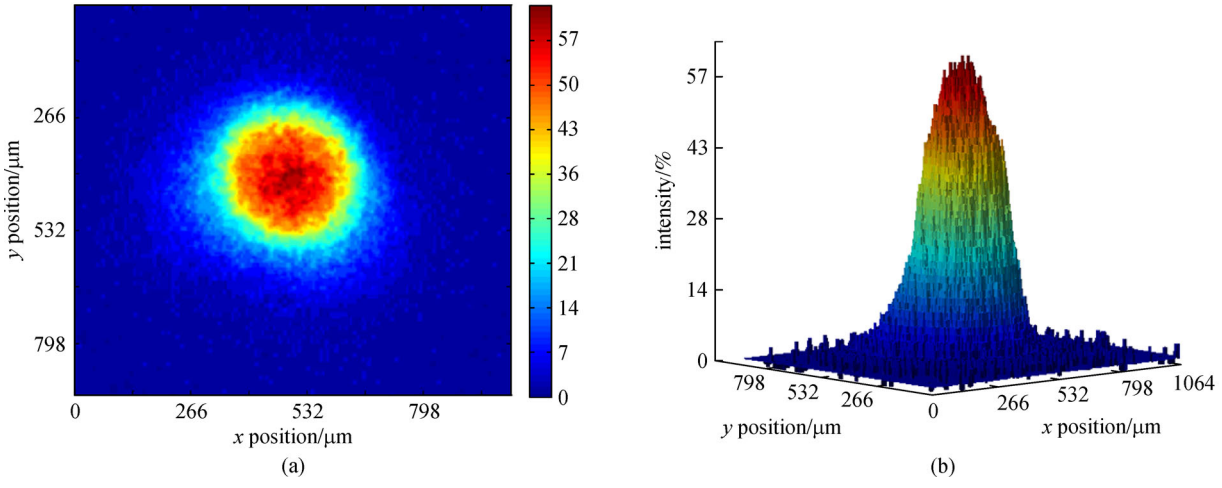

Fig. 10 (a) 2-D and (b) 3-D profiles of the reflected laser beam recorded in case of W1 (c = 0.130 m^{-1})

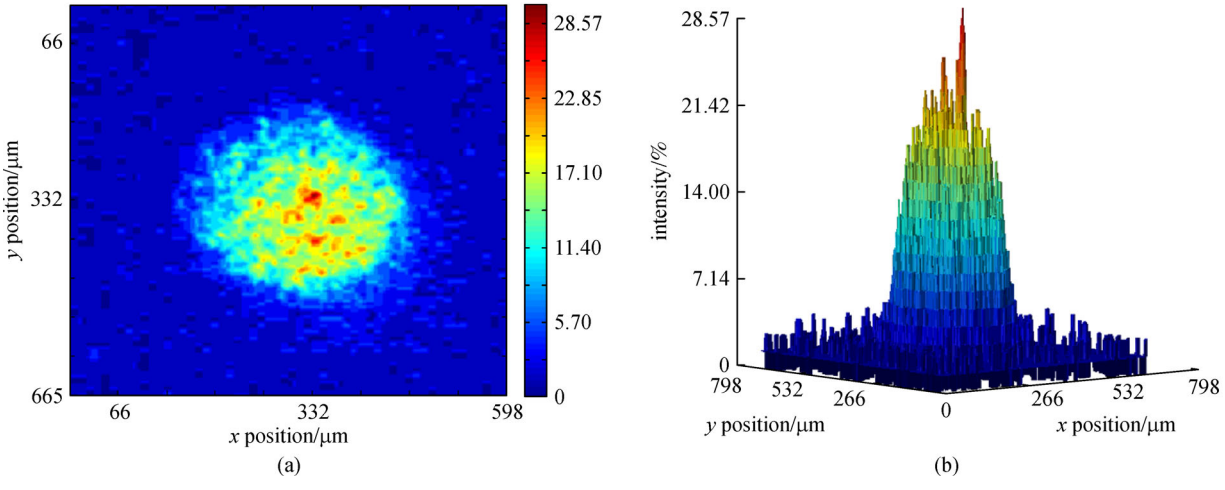

Fig. 11 (a) 2-D and (b) 3-D profiles of the reflected laser beam recorded in case of W2 (c = 0.343 m^{-1})

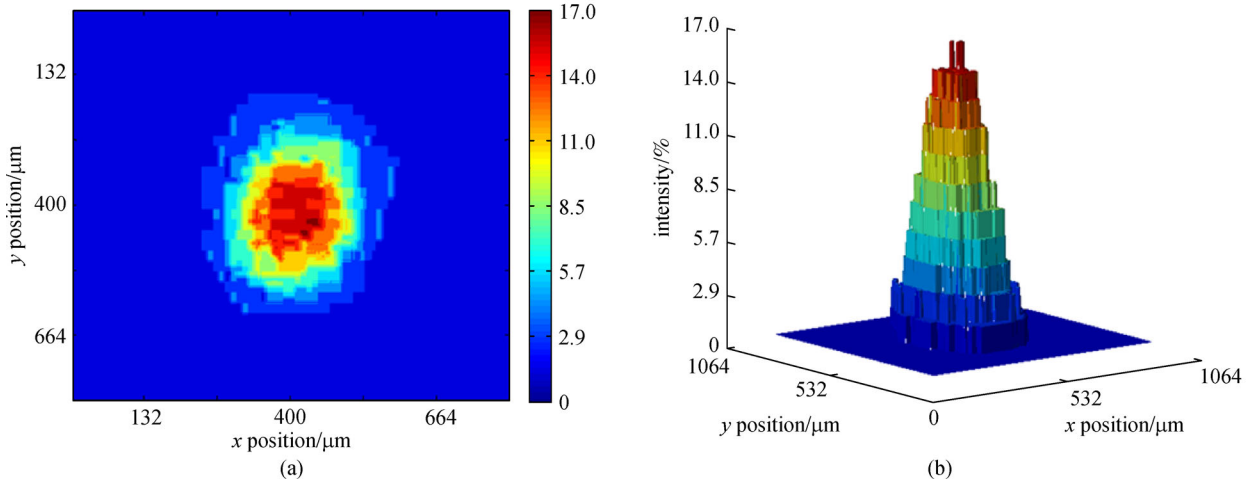

Fig. 12 (a) 2-D and (b) 3-D profiles of the reflected laser beam recorded in case of W3 (c = 0.580 m^{-1})

each water type. This leads us to conclude that the implemented optical model within Zemax software reproduces well the conditions of light propagation in a real underwater environment.

5 Conclusions

In this paper, the underwater light propagation was investigated by simulation and experiment. The Zemax-ray tracing software allowed us to simulate the light propagation and to observe the receiver response of a laser range finder in underwater environment. This latter was reproduced experimentally by adding different amounts of sand to tap water. Three types of water (W1, W2, and W3) were obtained with different attenuation coefficients (0.133, 0.343, 0.580 m^{-1}). It was observed that the three water types result in different transmitted laser powers and the experimental data validate those obtained from simulations. Therefore, the conclusion that can be drawn is that Zemax software can be effectively used to assess the light propagation in underwater environment by reproducing the appropriate water type, the receiver optics, and the laser source.

References

1. Wan D Z, Chin C S. Simulation and prototype testing of a low-cost ultrasonic distance measurement device in underwater. Journal of Marine Science and Technology, 2015, 20(1): 142–154
2. Grelowska G, Kozaczka E, Kozaczka S, Szymczak W. Gdansk Bay sea bed sounding and classification of its results. Polish Maritime Research, 2013, 20(3): 45–50
3. Cho H, Gu J, Joe H, Asada A, Yu S C. Acoustic beam profile-based rapid underwater object detection for an imaging sonar. Journal of Marine Science and Technology, 2015, 20(1): 180–197
4. Molebny V, McManamon P, Steinvall O, Kobayashi T, Chen W. Laser radar: historical prospective—from the East to the West. Optical Engineering (Redondo Beach, Calif.), 2016, 56(3): 031220
5. Huang Y, Cao F, Jin W, Qiu S. Underwater pulsed laser range-gated imaging model and its effect on image degradation and restoration. Optical Engineering (Redondo Beach, Calif.), 2013, 53(6): 061608
6. Rumbaugh L K, Bollt E M, Jemison W D, Li Y F. A 532 nm chaotic Lidar transmitter for high resolution underwater ranging and imaging. In: Proceedings of Oceans-San Diego. San Diego: IEEE, 2013
7. Szulwic J, Burdziakowski P, Janowski A, Przyborski M, Tysiąc P, Wojtowicz A, Kholodkov A, Matysik K, Matysik M. Maritime laser scanning as the source for spatial data. Polish Maritime Research, 2015, 22(4): 9–14
8. Khairi M T M, Ibrahim S, Yunus M A M, Faramarzi M, Yusuf Z. Artificial neural network approach for predicting the water turbidity level using optical tomography. Arabian Journal for Science and Engineering, 2016, 41(9): 3369–3379
9. Simileanu M, Radvan R, Puscas N. Underwater LIBS investigations setup for metals' identification. University Politehnica Of Bucharest Scientific Bulletin-Series A–Applied Mathematics And Physics, 2010, 72(4): 209–216
10. Wojtanowski J, Mierczyk Z, Zygmunt M. Laser remote sensing of underwater objects. In: Proceedings of SPIE Remote Sensing of the Ocean, Sea Ice, and Large Water Regions. Cardiff, Wales: SPIE, 2008
11. Zeng X, Xia M, Cheng Z, Li L, Chen J, Du P, Yang K. A small-size pulsed Lidar designed for obstacles detection in natural underwater environment. In: Proceedings of Applied Optics and Photonics China (AOPC2015). Beijing: International Society for Optics and Photonics, 2015
12. Amann M C, Bosch T M, Lescure M, Myllylae R A, Rioux M. Laser ranging: a critical review of usual techniques for distance measurement. Optical Engineering (Redondo Beach, Calif.), 2001, 40(1): 10–19
13. Osche G R. Optical detection theory for laser applications. In: Osche G R, ed. Optical Detection Theory for Laser Applications. New

York: Wiley-VCH, 2002, 424
14. Jelalian A V. Laser Radar Systems. New York: Artech House: 1992
15. Jerlov N. Classification of sea water in terms of quanta irradiance. Journal du Conseil, 1977, 37(3): 281–287
16. Mobley C D. Light and Water: Radiative Transfer in Natural Waters. San Diego: Academic press: 1994
17. Morel A. Optical properties of pure water and pure sea water. Optical aspects of oceanography, 1974, 1: 1–24
18. Smith R C, Baker K S. Optical properties of the clearest natural waters (200−800 nm). Applied Optics, 1981, 20(2): 177–184
19. Boivin L P, Davidson W F, Storey R S, Sinclair D, Earle E D. Determination of the attenuation coefficients of visible and ultraviolet radiation in heavy water. Applied Optics, 1986, 25(6): 877–882
20. Sverdrup H U, Johnson M W, Fleming R H. The Oceans: Their Physics, Chemistry, and General Biology. New York: Prentice-Hall Inc., 1942, Vol. 7
21. Zemax Development Corporation. Zemax 13 Optical Design Program User's Manual. 2014
22. Song Y, Chen Y, Xin J, Sun T. Two-dimensional beam shaping and homogenization of high power laser diode stack with rectangular waveguide. Frontiers of Optoelectronics, 2018, https://doi.org/10.1007/s12200-018-0831-z
23. Campazas A A, Cid M X A. Non-sequential modeling of commercial dichroic beamsplitters using Zemax. In: Proceedings of SPIE 9626, Optical Systems Design 2015: Optical Design and Engineering VI. Jena: SPIE, 2015, 96260C

Fatah Almabouada received the State Engineer degree (1997) and the Master degree (2013) in Electrical Engineering and is currently a Ph.D. student in Physics at Univérsité Kasdi Merbah Ouargla. At the Centre de Développement des Technologies Avancées (CDTA), he works at the Laser Systems Technologies Team (Ionized Medea and Lasers Division). His research interests include solid-state lasers and applications, optical design and optical instrumentation.

Manuel Adler Abreu has a degree in Physics and Materials Engineering (1989) and a Ph.D. degree in Physics Engineering (1996). At Faculdade de Ciências da Universidade de Lisboa Campus do Lumiar (FCUL), he works at the Laboratory of Optics, Lasers and Systems, and is coordinator of the Thematic Line of Instrumentation at the Institute of Astrophysics and Space Sciences. His research interests include optical instrumentation, sensors and optical metrology systems.

João M. P. Coelho has a degree in Physics and Materials Engineering (1992) and a Ph.D. degree in Physics Engineering (2003). At Faculdade de Ciências da Universidade de Lisboa Campus do Lumiar (FCUL), he works at the Laboratory of Optics, Lasers and Systems, and is coordinator of the Thematic Line Cancer Therapy and Drug Delivery at the Institute of Biophysics and Biomedical Engineering. His research interests include laser interaction with matter, biophysics, optical design and optical metrology. In these areas, he has published more than 90 articles in books, journals and proceedings. He has been, and is, project leader, task responsible or just team member in several international projects.

Kamal Eddine Aiadi received his B.S degree in Physics from Batna University (Algeria) and his Master degree from Bridgeport University (USA). He received his Ph.D. degree from Batna University (Algeria). Since 1987, he is a teacher at the Univérsité Kasdi Merbah Ouargla, and researcher, in LENREZA laboratory, at the same university. His research interests include optics, sensors, lasers and renewable energy.